A Comparison of Exact and Approximate Adjoint Sensitivities in Fluorescence Tomography

M. J. Eppstein*, F. Fedele, J. Laible, C. Zhang, A. Godavarty, and E. M. Sevick-Muraca

***Abstract*—Many approaches to fluorescence tomography utilize some form of regularized nonlinear least-squares algorithm for data inversion, thus requiring repeated computation of the Jacobian sensitivity matrix relating changes in observable quantities, such as emission fluence, to changes in underlying optical parameters, such as fluorescence absorption. An exact adjoint formulation of these sensitivities comprises three terms, reflecting the individual contributions of 1) sensitivities of diffusion and decay coefficients at the emission wavelength, 2) sensitivities of diffusion and decay coefficients at the excitation wavelength, and 3) sensitivity of the emission source term. Simplifying linearity assumptions are computationally attractive in that they cause the first and second terms to drop out of the formulation. The relative importance of the three terms is thus explored in order to determine the extent to which these approximations introduce error. Computational experiments show that, while the third term of the sensitivity matrix has the largest magnitude, the second term becomes increasingly significant as target fluorophore concentration or volume increases. Image reconstructions from experimental data confirm that neglecting the second term results in overestimation of sensitivities and consequently overestimation of the value and volume of the fluorescent target, whereas contributions of the first term are so low that they are probably not worth the additional computational costs.**

***Index Terms*—Adjoint sensitivities, fluorescence tomography, Jacobian matrices, frequency domain photon migration.**

I. Introduction

In recent years there has been increasing interest in the potential of fluorescence tomography as a means for molecularly-based noninvasive imaging in biological tissues [1]–[26]. By tagging regions of interest with target-specific fluorescing molecular probes [27]–[29], fluorescence tomography may enable estimation of three-dimensional (3-D) locations and geometries of target areas, such as tumors. We restrict this paper to discussions of frequency-domain fluorescence tomography, although the results may be readily applied to time-domain fluorescence tomography *via* Fourier transforms.

Frequency-domain fluorescence tomography in tissues requires 1) an accurate forward model of coupled excitation and emission light propagation through highly scattering media, and 2) a method for inverting measurements of emission phase-delays and/or amplitude attenuation to reconstruct interior optical property maps of the tissues. Comparisons of predictions from our forward model (a finite-element implementation of a diffusion model of coupled light propagation) to experimental measurements are discussed elsewhere [6]; the emphasis in this paper is on aspects of computing Jacobian sensitivities for image reconstruction. Because of the high degree of scattering and low signal-to-noise ratios, approaches to fluorescence tomography in large phantom volumes are typically based on regularized nonlinear least-squares optimization, such as the Levenberg–Marquardt method [8] or the Bayesian approximate extended Kalman filter [5]. Central to these methods is the repeated computation of Jacobian sensitivity matrices quantifying the effects of local changes in optical properties on the detected fluence. For such nonlinear least-squares-based approaches, the accuracy and computational efficiency of the Jacobian sensitivity matrices are fundamental to the overall accuracy and computational efficiency of the tomographic reconstructions.

Various approaches to computing emission sensitivities that have been applied to fluorescence tomography include first-order finite differences [3], second-order finite differences [4], an approximate adjoint approach that assumes smoothness and linearity [5], [7], [8], and an exact adjoint approach [6], [33]. The finite-difference approaches are flexible and accurate but can be prohibitively slow, especially when a large finite-element forward model is employed. Adjoint approaches to calculating sensitivities [30], [31] have long been used in a variety of inverse problems to speed up sensitivity calculations, including in diffuse optical tomography of endogenous optical properties [32]. However, in fluoresence tomography the uni-directional coupling between excitation and emission light propagation complicates the adjoint formulation considerably [33]. Approximations that limit this coupling can further improve the computational efficiency of the adjoint approach, but should only be used if the approximations do not significantly affect accuracy. In this paper, we examine the importance of the three terms comprising the exact adjoint sensitivity formulation for computing the sensitivity of frequency-domain emission measurements with respect to fluorescence absorption, and the effects of making simplifying assumptions regarding 1) smoothness of the diffusion coefficient and 2) linearity of the

Manuscript received January 13, 2003; revised June 5, 2003. This work was supported by the National Institutes of Health (NIH) under Grant R01 EB 002763. The Associate Editor responsible for coordinating the review of this paper and recommending its publication was A. Hielscher. *Asterisk indicates corresponding author.*

*M. J. Eppstein is with the Department of Computer Science, University of Vermont, Votey Bldg., 33 Colchester Ave., Burlington, VT 05405 USA (e-mail: Maggie.Eppstein@uvm.edu).

F. Fedele and J. Laible are with the Department of Civil & Environmental Engineering, University of Vermont, Burlington, VT 05405 USA.

C. Zhang is with the Department of Computer Science, University of Vermont, Burlington, VT 05405 USA.

A. Godavarty and E. M. Sevick-Muraca are with the Photon Migration Laboratories, Department of Chemical Engineering, Texas A&M University, College Station, TX 77843-3573 USA.

Digital Object Identifier 10.1109/TMI.2003.818165

sensitivity with respect to fluorescence absorption. We report on computational experiments showing how the accuracy of exact and approximate formulations, that omit one or more terms, differ with varying amounts of fluorophore in the domain, and we examine the effects of using linearity approximations on image reconstruction from experimental data collected on a breast-mimicking phantom.

II. Governing Equations

The generation and propagation of fluorescent light through highly-scattering media (such as biological tissues) is often modeled by a pair of second order, coupled, elliptic, partial differential equations [34]–[36]. The first equation represents propagation of excitation light (subscript x) and the second models the generation and propagation of fluorescently emitted light (subscript m). In the frequency domain, these diffusion approximations to the coupled radiative transport equation over a 3-D bounded domain Ω are

$$\begin{cases} -\nabla\cdot(D_x\nabla\Phi_x)+k_x\Phi_x=S_x \\ -\nabla\cdot(D_m\nabla\Phi_m)+k_m\Phi_m=\beta\Phi_x \end{cases} \text{on } \Omega \tag{1}$$

subject to the Robin boundary conditions on the domain boundary $\partial\Omega$ of

$$\begin{cases} \overrightarrow{n}\cdot(D_x\nabla\Phi_x)+b_x\Phi_x=0 \\ \overrightarrow{n}\cdot(D_m\nabla\Phi_m)+b_m\Phi_m=0 \end{cases} \text{on } \partial\Omega \tag{2}$$

where ∇ is the 3×1 gradient operator and $\overrightarrow{n}$ is the 3×1 vector normal to the boundary. The excitation light source S_x (W/cm^3) is intensity modulated with sinusoidal frequency ω(rad/s), and propagates through the media resulting in the ac component of complex photon fluence at the excitation wavelength of Φ_x (W/cm^2), where $\Phi_x = A_x e^{i\theta_x}$ with ac amplitude A_x and phase θ_x. Some of this excitation light may be absorbed by fluorophore in the media and reemitted, resulting in complex photon fluence at the emission wavelength $\Phi_m = A_m e^{i\theta_m}$. The diffusion $(D_{x,m})$, decay (k_x, m), and emission source (β) coefficients, as shown below

$$\begin{aligned} D_x &= \frac{1}{3\,(\mu_{axi}+\mu_{axf}+\mu'_{sx})} \\ D_m &= \frac{1}{3\,(\mu_{ami}+\mu_{amf}+\mu'_{sm})} \\ k_x &= \frac{i\omega}{c}+\mu_{axi}+\mu_{axf} \\ k_m &= \frac{i\omega}{c}+\mu_{ami}+\mu_{amf} \\ \beta &= \frac{\phi\mu_{axf}}{1-i\omega\tau} \end{aligned} \tag{3}$$

are functions of absorption due to nonfluorescing chromophore (μ_{axi}, μ_{ami}), absorption due to fluorophore (μ_{axf}, μ_{amf}), and isotropic (reduced) scattering (μ'_{sx}, μ'_{sm}) at the two wavelengths (all in units of cm^{-1}), fluorescence quantum efficiency (ϕ), and fluorescence lifetime (τ,in s). Here, $i=\sqrt{-1}$, and c is the speed of light in the medium (cm/s). The Robin boundary coefficients (b_x, b_m) are governed by the reflection coefficients (R_x, R_m), which range from 0 (no reflectance) to 1 (total reflectance)

$$b_x = \frac{1-R_x}{2(1+R_x)}; \quad b_m = \frac{1-R_m}{2(1+R_m)}. \tag{4}$$

Fluorescence absorption at the emission wavelength μ_{amf} is related to fluorescence absorption at the excitation wavelength μ_{axf} by the ratio of their extinction coefficients ($\epsilon_{am} = 11\,000\ M^{-1}\text{cm}^{-1}$, $\epsilon_{ax} = 130\,000\ M^{-1}\text{cm}^{-1}$), so $\mu_{amf} = 0.0846\cdot\mu_{axf}$. Thus, when we estimate μ_{axf} we are also implicitly estimating μ_{amf}. Although not explicitly shown in these equations, all optical properties are understood to be potentially variable in Cartesian space.

III. Adjoint Sensitivity Formulation

Fedele *et al.* [33] have derived the exact adjoint solution for sensitivities of emission fluence in the coupled system with respect to any underlying optical property p, with the following result:

$$\begin{aligned} \delta\Phi_m = &-\int_\Omega \nabla\Psi_{mm}\frac{\partial D_m}{\partial p}\delta p\nabla\Phi_m - \int_\Omega \Psi_{mm}\frac{\partial k_m}{\partial p}\delta p\Phi_m \\ &-\int_{\partial\Omega}\Psi_{mm}\frac{\partial b_m}{\partial p}\delta p\Phi_m - \int_\Omega \nabla\Psi_{xm}\frac{\partial D_x}{\partial p}\delta p\nabla\Phi_x \\ &-\int_\Omega \Psi_{xm}\frac{\partial k_x}{\partial p}\delta p\Phi_x - \int_{\partial\Omega}\Psi_{xm}\left(\frac{\partial b_x}{\partial p}\delta p\Phi_x\right) \\ &+\int_\Omega \Psi_{mm}\frac{\partial\beta}{\partial p}\delta p\Phi_x. \end{aligned} \tag{5}$$

where the adjoint variables Ψ_{xm} and Ψ_{mm} must satisfy

$$-\nabla\cdot(D_m\nabla\Psi_{mm})+k_m\Psi_{mm}=\Delta_d \quad \text{on } \Omega \tag{6a}$$

$$-\nabla\cdot(D_x\nabla\Psi_{xm})+k_x\Psi_{xm}=\beta\Psi_{mm} \quad \text{on } \Omega \tag{6b}$$

where Δ_d is the Dirac impulse function at some set of detectors d, subject to

$$\begin{cases} \vec{n}\cdot(D_m\nabla\Psi_{mm})+b_m\Psi_{mm}=0 \\ \vec{n}\cdot(D_x\nabla\Psi_{xm})+b_x\Psi_{xm}=0 \end{cases} \text{on } \partial\Omega. \tag{7}$$

In our implementation of the adjoint method, we employ analytic expressions for the derivatives in (5). For example, the analytic expression for $\partial D_x/\partial\mu_{axf}$ is

$$\frac{\partial D_x}{\partial\mu_{axf}} = -\frac{1}{3(\mu_{axi}+\mu_{axf}+\mu'_{sx})^2}. \tag{8}$$

The relative magnitudes of the terms in (5) depend on which parameter p is selected as well on the current parameter values of p. For $p\equiv\mu_{axf}$, the derivatives of the boundary terms b_x and b_m may be assumed to be 0, and so for this particular case (5) simplifies to

$$\begin{aligned} \delta\Phi_m = &-\int_\Omega\left(\nabla\Psi_{mm}\frac{\partial D_m}{\partial\mu_{axf}}\delta\mu_{axf}\nabla\Phi_m\right. \\ &\left.-\Psi_{mm}\frac{\partial k_m}{\partial\mu_{axf}}\delta\mu_{axf}\Phi_m\right) \qquad (9a) \\ &-\int_\Omega\left(\nabla\Psi_{xm}\frac{\partial D_x}{\partial\mu_{axf}}\delta\mu_{axf}\nabla\Phi_x\right. \\ &\left.-\Psi_{xm}\frac{\partial k_x}{\partial\mu_{axf}}\delta\mu_{axf}\Phi_x\right) \qquad (9b) \\ &+\int_\Omega\Psi_{mm}\frac{\partial\beta}{\partial\mu_{axf}}\delta\mu_{axf}\Phi_x. \qquad (9c) \end{aligned}$$

It has been proposed [7], [8] to make the simplifying assumption that $\delta\Phi_m$ is linear with respect to μ_{axf}, although the magnitude of the impact of this linearity assumption on the accuracy of the approximated sensitivities has not previously been analyzed. Implicit in this linearity assumption are the assumptions that the diffusion and decay coefficients are independent of fluorescence absorption. If one assumes that D_m and k_m are independent of μ_{axf}, the first term (9a) goes to zero. If one assumes that D_x and k_x are independent of μ_{axf}, the second term (9b) goes to zero. Another simplification that has been employed [7], [8] is to assume that D_m is spatially smooth (and hence $\nabla D_m = 0$), although this assumption warrants questioning [37]. If D_m is assumed to be smooth, the emission equation can be divided by D_m and simplified to

$$-\nabla^2\Phi_m + \frac{k_m}{D_m}\Phi_m \approx \frac{\beta\Phi_x}{D_m}. \tag{10}$$

The Green's function G_m for the modified emission (10) can then be found by solving

$$-\nabla^2 G_m + \frac{k_m}{D_m}G_m = \Delta_d. \tag{11}$$

This Green's function G_m is related to the adjoint variable Ψ_{mm} as follows:

$$\frac{G_m}{D_m} \underset{\nabla D_m \to 0}{\overset{\lim}{\Longrightarrow}} \Psi_{mm}.$$

Consequently, if one assumes that D_m is smooth, the third term (9c) collapses to

$$\int_\Omega \frac{G_m \phi \Phi_x}{D_m(1 - i\omega\tau)}\delta\mu_{axf} \tag{12}$$

where we have substituted the analytic derivative for $\partial\beta/\partial\mu_{axf}$. Term (12) is identical to an approximate adjoint formulation previously employed for estimating $\partial\Phi_m/\partial\mu_{axf}$ [5], [7], [8]. In the next two sections, we examine the relative importance of the contribution of each of the three terms (9a)–(9c) of the exact sensitivity formulation to the sensitivity of emission fluence with respect to fluorescence absorption, and the impact of the linearity and smoothness assumptions on image reconstructions of fluoresence absorption from emission fluence in fluorescence tomography.

IV. Contribution of Terms in Adjoint Sensitivities

In the previous section, we showed that the sensitivity equation for emission fluence with respect to fluorescence absorption is shown to comprise three distinct terms. Term 1 (9a) reflects contributions of the sensitivities of the diffusion and decay coefficients at the emission wavelength, Term 2 (9b) reflects contributions of the diffusion and decay coefficients at the excitation wavelength, and Term 3 (9c) reflects the contribution of the sensitivity of the emission source term. We conducted computational experiments using a finite-element implementation [33] to better understand the relative contributions of these three terms.

A. Design of Computational Experiments

In order to compare the accuracy and efficiency of the various methods for computing the sensitivities, we compared results on a $4 \times 8 \times 8$ cm^3 synthetic domain, with coordinate ranges $\langle -2 \cdots 2, -4 \cdots 4, -4 \cdots 4\rangle$ cm (Fig. 1). The size, shape, and optical properties of this domain were similar to those of an existing experimental tissue-mimicking phantom used for experiments in fluorescence tomography using the fluorophore indocyanine green [5], with excitation $\lambda = 785$ nm and emission $\lambda = 830$ nm at $\omega = 100$ MHz modulation frequency. Background optical properties were modeled as homogeneous with the following values: $\mu_{axf} = 0.006$ cm^{-1}, $\mu_{amf} =$ 5.06e-4 cm^{-1}, $\mu_{axi} = 0.031$ cm^{-1}, $\mu_{ami} = 0.0415$ cm^{-1}, $\mu'_{sx} = 10.95$ cm^{-1}, $\mu'_{sm} = 9.29$ cm^{-1}, $\tau = 0.56$ ns, $\phi = 0.016$. Boundary reflection coefficients were selected to be $R_{x,m} =$ 0.431 on the top at the air/liquid interface, and $R_{x,m} = 0.0222$ on the other five sides for the acylic/liquid interfaces [38]. The mesh used for these experiments had 2601 nodes and 12 288 elements, with 0.25-cm spacing between nodes. A spherical fluorescing target was modeled in the center of the domain at $\langle 0, 0, 0\rangle$ cm. We ran two sets of experiments. In one set of experiments, we simulated a large 3-cm diameter target, with target:background contrast in μ_{axf} varying from no contrast to 400:1 contrast. In the second set of experiments, we simulated a strongly fluorescing target (400:1 target:background contrast in μ_{axf}) with varying diameters from 1 to 3 cm. These ranges were deliberately chosen to represent extreme values, in order to more clearly elucidate trends. All other optical properties were assumed homogeneous throughout the domain. In both sets of experiments, we simulated point illumination with excitation at surface location $\langle -2, -1, 1\rangle$. Sensitivities vary by orders of magnitude across large domains [33], so it is difficult to illustrate differences between approximated sensitivities simultaneously over large portions of the domain. Consequently, we report the sensitivities of emission fluence

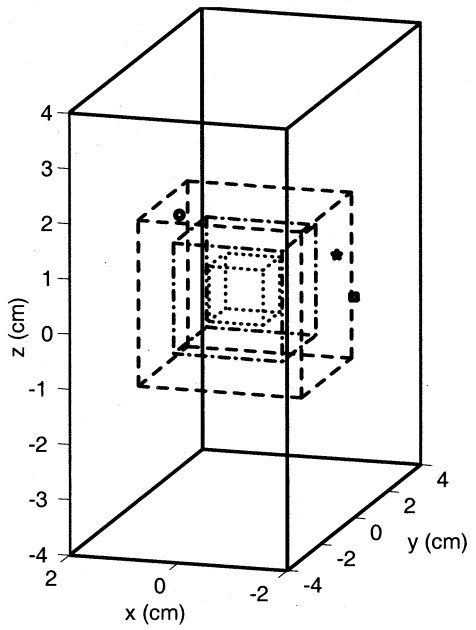

Fig. 1. The $4 \times 8 \times 8$ cm^3 simulated domain. Target sizes and locations are shown for a 1-cm diameter target (dotted), a 2-cm diameter target (dash-dotted), and a 3-cm diameter target (dashed). Sensitivities reported herein are for emission fluence at the black square on the surface, with respect to fluorescence absorption at the internal node marked with a black circle, in reponse to a surface excitation light source at the black star.

at a surface detector located at $\langle -2, 0, 0 \rangle$ cm, with respect to changes in fluorescence absorption at an internal node at $\langle 1.5, 1, 1 \rangle$ cm. These locations were arbitrarily selected as representative of values relatively sensitive to changes in the target fluorophore, as a means of illustrating the magnitude of differences that can occur. The relative locations of 1-, 2-, and 3-cm diameter targets, and the locations of the source, detector, and designated internal node are shown in Fig. 1. In addition to the representative sensitivity values reported here, in Section V we assess the impact of various approximations to the sensitivities on tomographic reconstructions of fluorescence absorption over an entire phantom domain.

B. Results of Computational Experiments

In Fig. 2, we show the real and imaginary parts of the designated sensitivities for both sets of experiments as "fence" diagrams showing two vertical cross sections through the 3-D space. In the left portion of each panel, we show the change in sensitivity as a function of changing the diameter of a target with 400:1 contrast in μ_{axf}, while in the right portions we show the change in sensitivity as a function of changing the contrast of a large 3-cm diameter target. From Fig. 2, it is apparent that as the amount of fluorophore increases (due to greater concentration of fluorophore in the target and/or larger diameter of the target), the magnitude of exact emission sensitivity (solid line) decreases. This decrease is due, in part, to a decrease in the magnitude of Term 3 (caused by a decrease in the magnitude of excitation fluence). However, both the magnitude and relative contributions of Terms 1 and 2 (especially the latter) to the overall sensitivity increase as the amount of fluorophore increases and, since the sign of these terms is opposite to the sign of Term 3, they further contribute to the reduction in the magnitude of the overall sensitivity.

The change in relative importance of the various terms can be seen more clearly in Fig. 3. Here, the contributions of the absolute values of the real and imaginary parts of each of the three terms are plotted relative to the sums of the absolute values of the real and imaginary parts of all three terms. Relative contributions of real and imaginary parts vary similarly (Fig. 3), although the signs of these components are opposite (Fig. 2). When there is no contrasting target, the average relative contributions of Terms 1, 2, and 3, are 0.1%, 1.3%, and 98.6%, respectively. However, with a large (3-cm diameter), highly absorbing (400:1 contrast) target, the relative contributions are 6.9%, 35.3%, and 57.8%.

With homogeneous scattering, even when fluorescence absorption contrast was 400:1 in the target, the approximation (12) due to the joint assumptions of linearity and smoothness was coincident with Term 3 of the full adjoint solution (9c). However, when we also varied scattering within the target, we were able to detect small differences between these two terms. For example, in a 2-cm diameter target with 100:1 contrast in absorption due to fluorophore and 2:1 contrast in scattering over background, the approximation (12) differed by 3.5% from Term 3 of the full adjoint solution (9c), reflecting the error introduced by the assumption that $\nabla D_m = 0$. It should be noted, however, that introduction of exogenous fluorophore will not introduce additional scattering contrast into targets.

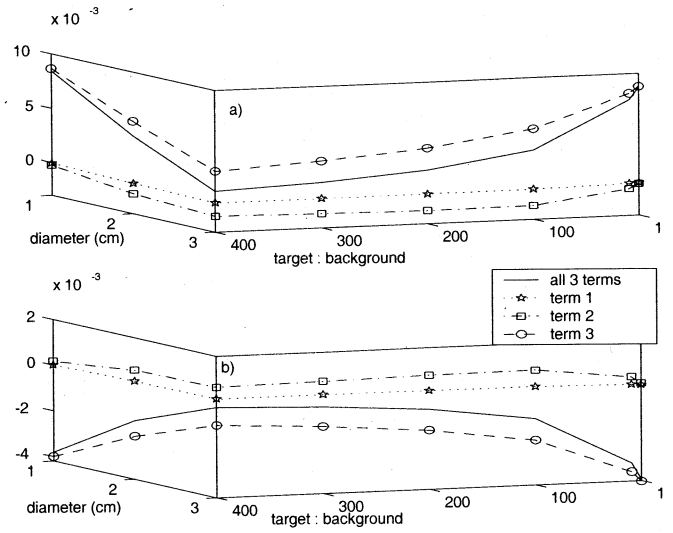

Fig. 2. Real (a) and imaginary (b) parts of the exact adjoint sensitivity, and its component three terms (9a)–(9c), of emission fluence with respect to fluorescence absorption at the locations shown in Fig. 1. These results are depicted with fence diagrams showing two vertical cross sections through the 3-D space. In the left portion of each panel, we show the change in sensitivity as a function of changing the diameter of a target with 400:1 target:background constrast in μ_{axf}, while in the right portions we show the change in sensitivity as a function of changing the contrast in μ_{axf} of a large 3-cm diameter target.

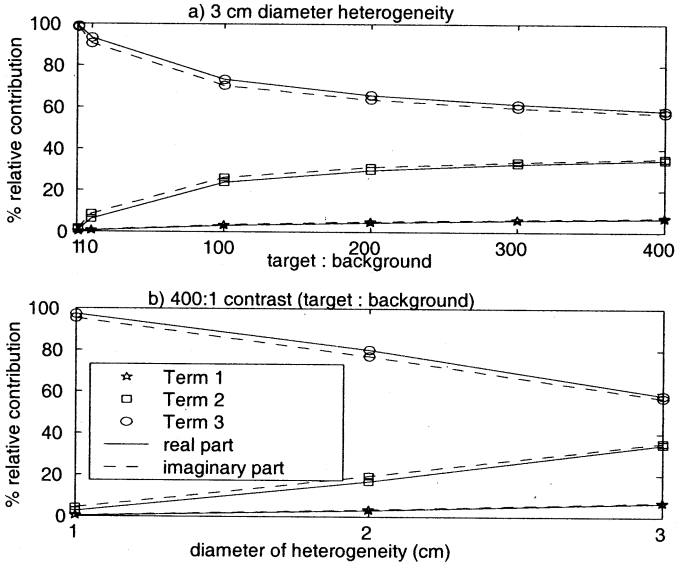

Fig. 3. The contribution of each of the three terms (9c)–(9c) to the overall sensitivity shown in Fig. 2 as a) contrast in fluorescence absorption is varied and b) diameter of the fluorescent target is varied, for a fluorescing target located in the center of the domain.

Thus, our computational experiments for the sensitivities of emission fluence with respect to fluorescence absorption show that when there is little fluorescence absorption in the domain, Term 3 [or its approximation, term (12)] accounts for nearly all the sensitivity of emission fluence. Making the assumption that $\nabla D_m = 0$ introduces only a small error into absorption sensitivities, even when scattering is discontinuous, but since there are also no computational gains to be reaped from making such an assumption we see no justification for doing so. Omitting Term 2 would save the computation required for (9b), but more

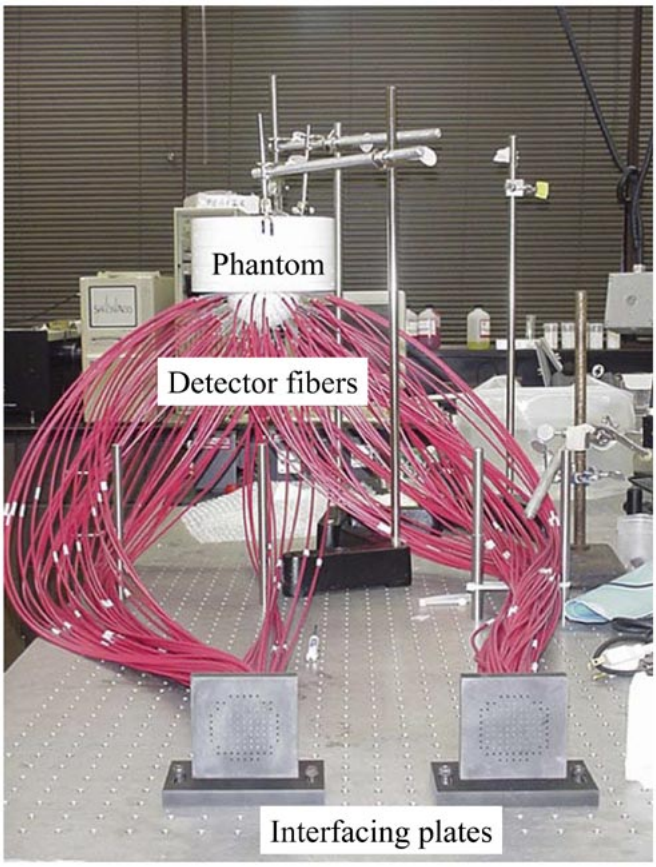

Fig. 4. The shape of the phantom is a 10-cm diameter hemispherical "breast" attached to a 20-cm diameter cylindrical portion of the "chest wall." The phantom is constructed from a PVC shell filled with 1087 cc of a 1% Liposyn solution. There are 128 symmetically placed detector fibers attached to the hemisphere and mounted on interfacing plates, where they are imaged using an ICCD camera for detection of phase and amplitude.

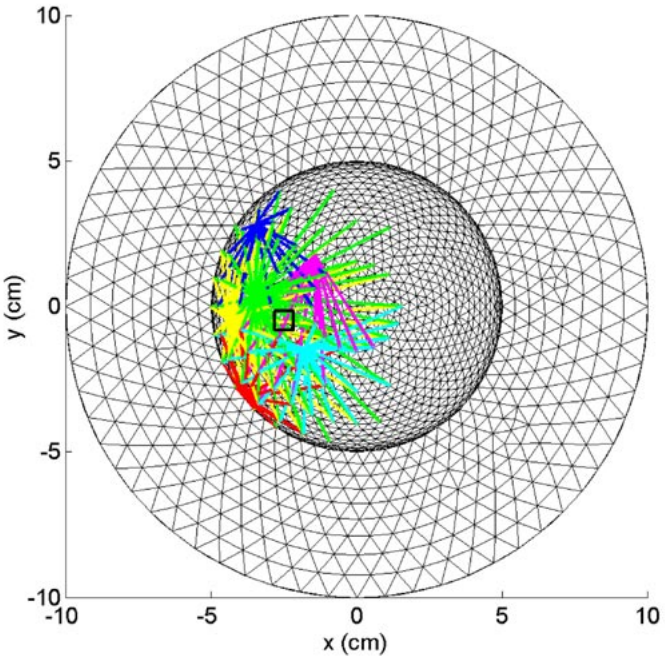

Fig. 5. A top view of the 43 313-element (6956 node) model of the breast-shaped phantom. Each retained source-detector pair (see text) is shown colored by source; the convex hull of these rays approximates the portion of the domain that is sampled by the measurements used in the reconstruction. The x-y location of the fluorescent heterogeneity centered at $\langle -2.5, -0.5, 2.5 \rangle$ is indicated by the black square.

significantly would also preclude the need to compute Ψ_{xm} with (6b). However, as fluorophore increases, the relative contribution of Term 2 becomes increasingly important. Omitting Term 1 would save the computation required for (9a), and the contribution of this term remains relatively low, even with very large amounts of fluorophore. In the next section we observe how omission of Terms 1 and 2 from the sensitivity calculation affects the accuracy of image reconstruction of fluorescence absorption from experimental data on a breast-mimicking phantom.

V. Effects of Adjoint Approximations on Fluorescence Tomography

A. Design of Phantom Experiments

In order to better appreciate the effects of the three terms in the adjoint emission sensitivities on fluorescence tomography, we reconstructed a fluorescent target from experimental measurements of phase and amplitude data collected on a tissue-mimicking phantom. Details of the tissue-mimicking phantom, instrumentation, and data collection methodology, are described in detail elsewhere [6]; for completeness, we outline them briefly here. The tissue mimicking phantom was constructed to model a 10-cm diameter hemispherical breast attached to a 20-cm diameter cylindrical portion of the chest wall (Fig. 4). This was modeled with a 3-D finite-element mesh, as shown in Figs. 5 and 6(b), with an average node spacing of 0.5 cm in the hemispherical portion of the model. The hollow phantom was filled with 1087 cm^3 of a 1% Liposyn solution with optical properties similar to that of normal human breast tissue [39] ($\mu_{axf} = 0.0$ cm^{-1}, $\mu_{amf} = 0.0$ cm^{-1}, $\mu_{axi} = 0.023$ cm^{-1}, $\mu_{ami} = 0.031$ cm^{-1}, $\mu'_{sx} = 10.18$ cm^{-1}, $\mu'_{sm} = 8.64$ cm^{-1}); a 1 cm^3 sealed cuvette containing 1 μM of Indocyanine green ($\mu_{axf} = 0.3$ cm, $\mu_{amf} = 0.0254$ cm^{-1}, $\tau = 0.56$ ns, $\phi = 0.016$) was suspended about 1 cm inside the surface of the "breast", at location $\langle -2.5, -0.5, 2.5 \rangle$ cm from the center of the base of the hemisphere, as indicated in Figs. 5 and 6(b). As there was no fluorophore added to the background, this models perfect uptake into a physiological target, such as a tumor or lymph node in a sentinel lymph node imaging application. A gain modulated-image intensified charge-coupled device (ICCD) camera was used to obtain the measurements in terms of ac and phase in the frequency domain [40]. A high power laser diode (375 mW, HPD1105-9mm-D-78 505 model, High Power Devices Inc., North Brunswick, NJ) modulated at 100 MHz was used to illuminate the phantom using up to 28 multimode optical fibers one at a time. Detection of emitted light occurred at 128 optical fibers located symmetrically on the hemispherical phantom surface. All these collection fibers are interfaced onto two plates (Fig. 4) in order to image multiple source-detector pairs simultaneously using the ICCD camera. The image intensifier (FS99001C Gen III model, ITT Industries Night Vision, Roanoke, VA) was also modulated at 100 MHz, making it a homodyned imaging system [26]. The

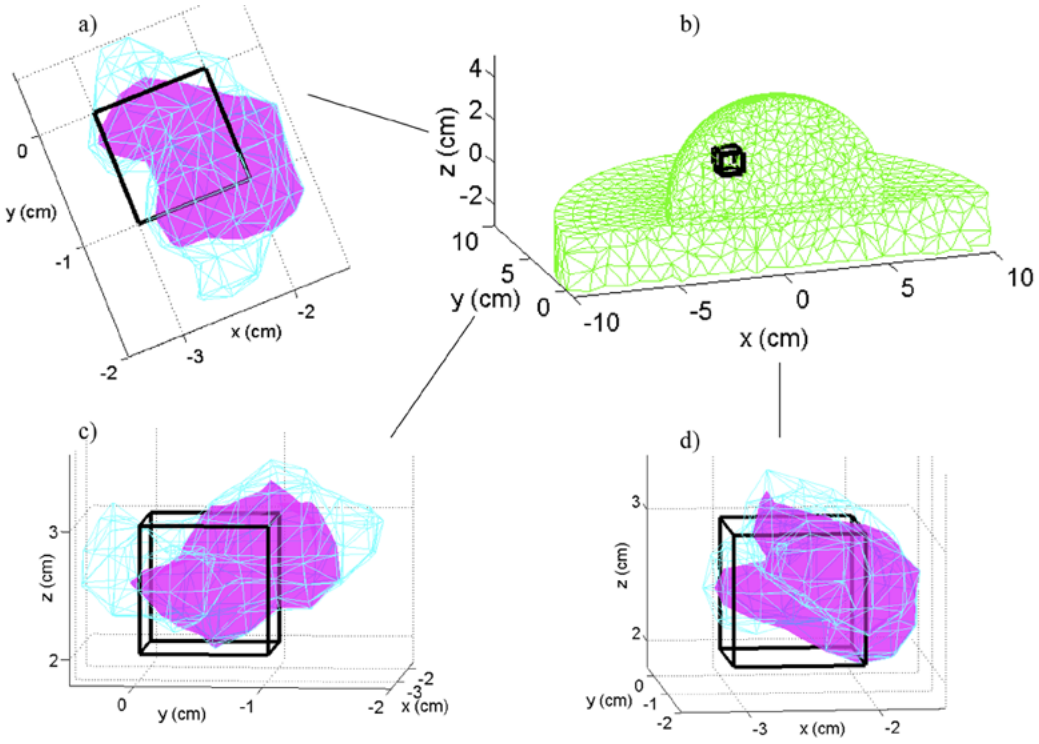

Fig. 6. A cross section of the finite-element mesh showing the true location of the 1 cm^3 fluorescent target is depicted in b. In (a), (c), and (d) we show three views from the perspectives of the z, y, and $x$axes, respectively, comparing the true target size and location (black cube) with the reconstruction of the target using the full adjoint Jacobian sensitivities (magenta solid) that includes Terms 1, 2, and 3 (9a)–(9c), and the approximate adjoint Jacobian sensitivities (cyan wire-frame) that only includes Term 3 (9c).

selection of sources and detectors used in the reconstruction was data-directed, as follows. Data was only recorded for source-plate pairs where the modulation depth (ac/dc) was greater than the noise floor of 0.1. In addition, individual source-detector measurements less than 0.025 were discarded, leaving a total of 384 source-detector pairs (from six source locations) used in the inversion. The x-y spatial coverage of the retained source-detector pairs is shown in Fig. 5, relative to the location of the target. Emission measurements used in the reconstruction were referenced to emission measurements at designated reference nodes to account for unknown source strength and instrument effects.

B. Image Reconstruction Algorithm

For image reconstruction we used a form of the Bayesian approximate extended Kalman filter; a stochastic, nonlinear, minimum-variance, least-squares estimator that requires the Jacobian sensitivity matrix to be recalculated during each iteration [3]–[6]. In any nonlinear least-squares parameter estimation algorithm, the heart of the algorithm is an update $\mathbf{\Delta p}$ of the following form:

$$\mathbf{\Delta p} = (\mathbf{J}^T \cdot \mathbf{W} \cdot \mathbf{J} + \mathbf{D})^{-1} \cdot \mathbf{J}^T \cdot \mathbf{W} \cdot (\mathbf{z} - \mathbf{x}) \qquad (13)$$

where $\mathbf{D}$ is a damping matrix (possibly $\mathbf{0}$), $\mathbf{W}$ is a weight matrix (possibly the identity matrix $\mathbf{I}$), $\mathbf{z}$ is a vector of measurements (here, log of ac ratio and relative phase shift of referenced emission fluence), $\mathbf{x}$ is a vector of predicted measurements, $\mathbf{p}$ is a vector of uncertain parameters (here a pseudobeta transform [3] of μ_{axf}), J is the appropriate Jacobian sensitivity matrix relating $\mathbf{x}$ and $\mathbf{p}$, and the superscript T is matrix transpose. For example, in the approximate extended Kalman filter, $\mathbf{W}$ is the inverse of the sum of the measurement error and model error covariances and $\mathbf{D}$ is the inverse of the recursively updated parameter error covariance. Measurement error variance was empirically determined from five repetitions of measurements for each source-detector pair, and model error variance was approximated by the inverse of modulation depth scaled to the order of computed model error from known domains. The reconstruction was determined to have converged when the sum of squared output error did not decrease by more than 1%.

Regardless of the choice of the weight and/or damping matrices, it is clear from (13) that in any nonlinear least-squares formulation the Jacobian $\mathbf{J}$ appears twice in the denominator and only once in the numerator of the update. In the case of fluorescence tomography, the sensitivity is always much less than 1.0, with the consequence that if the sensitivity is overestimated (but still less than 1.0), the nonlinear least-squares update of parameters $\mathbf{p}$ will also be overestimated.

C. Results of Image Reconstructions

Quality of target reconstruction was quantified by estimating the volume and volume-integrated fluorescence absorption of the reconstructed target. The spatial extent of the reconstructed target was determined by imposing a cutoff value between background and target values. We selected a cutoff value of fluorescence absorption of 0.1 cm^{-1}, based on the break between modes in the bimodal histogram of the reconstructed

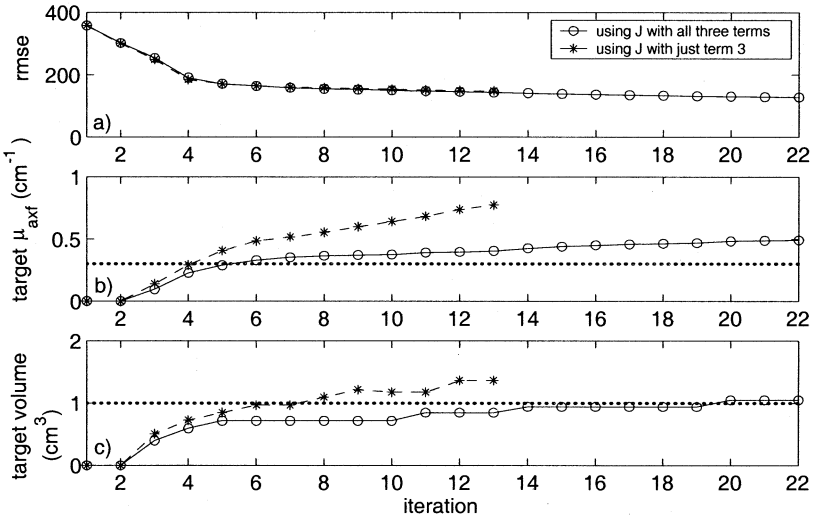

Fig. 7. (a) Reduction in root mean square error of $ln(\Phi_m)$; convergence was assumed when this quantity decreased by less than 1%. (b) Evolution of volume-integrated fluorescence absorption in the reconstructed target; true absorption is shown by the dotted line. (c) Evolution of the volume of the reconstructed target; true volume is shown by the dotted line.

distributed fluorescence absorption coefficients. Using this criterion, the reconstruction using the exact adjoint sensitivities that included all three terms (9a)-(9c) yielded a single fluorescent target with (volume integrated) fluorescence absorption of 0.49 cm^{-1} and volume of 1.05 cm^3. Three magnified views of this reconstructed target are shown by the magenta solid in Fig. 6(a), (c), and (d). This estimate of fluorescence absorption is higher than the true fluorescence absorption of 0.30 cm^{-1}, although the volume estimate is close to the actual size of 1.0 cm^3 of the fluorescent target (as shown by the black cube in Fig. 6). The overestimate of fluorescence absorption may be due to a variety of reasons, including parameter settings in the reconstruction algorithm, choice of target cutoff, and insensitivity of the convergence criterion to absolute absorption values. On the other hand, when using an approximate adjoint formulation that only includes the third term (9c) in the Jacobian, both the value and size of the target was markedly higher at 0.77 cm^{-1} and 1.37 cm^3, respectively, as shown by the cyan wire-mesh in Fig. 6(a), (c), and (d). As expected, a reconstruction that used only Terms 2 and 3 (not shown) was essentially identical to that using Terms 1, 2, and 3 and implies that Term 1 may be omitted from the sensitivity calculation without introducing significant error into the reconstruction, at least when the amount of fluorophore is in the range tested here. In all cases, the target was reconstructed in the correct location (Fig. 6), with the centroid being within a few millimeters of the true centroid location. Surprisingly, the root mean square error (rmse) of the predictions decreased similarly for reconstructions using both the exact and approximate (Term 3 only) adjoint sensitivities [Fig. 7(a)], although the more aggressive updates using the approximate adjoint sensitivities caused the reconstruction to converge more quickly, in 13 iterations rather than 22, where convergence is defined as before to be less than a 1% change in output rmse. The value and volume of the reconstructed target grew at a markedly faster rate when using the approximate vs. exact adjoint sensitivities, as shown in Fig. 7(b), (c). Fig. 7(a) highlights the insensitivity of the output rmse to changes in the fluorescence absorption estimate [Fig. 7(b)] and the limitations of using this metric to detect convergence (and, therefore, obtain quantitatively accurate estimates of fluorescence absorption) and to assess quality of the reconstruction.

TABLE I
COMPUTATION TIMES FOR ONE ITERATION

equation number	quantity computed	cpu time (s)
1	Φ_x and Φ_m	7.8
6a	Ψ_{mm}	13.5
6b	Ψ_{xm}	16.9
9a	Term 1	10.4
9b	Term 2	10.4
9c	Term 3	5.2
6a+6b+9	$\frac{\partial \Phi_m}{\partial \mu_{axf}}$ (using Terms 1+2+3)	56.4
6a+6b+14	$\frac{\partial \Phi_m}{\partial \mu_{axf}}$ (using Terms 2+3)	46.0
6a+9c	$\frac{\partial \Phi_m}{\partial \mu_{axf}}$ (using Term 3 only)	18.7

The required computation times per iteration are dependent on the number of sources, the number of detector locations, the size of the mesh, in addition to specifics of the software implementation and hardware platform. On this particular reconstruction, with six sources, 64 detector locations, 6956 nodes, and 34 413 elements in the mesh, using a vectorized implementation of the program in Matlab V. 6.1 [33], and running on a 2.2-GHz Pentium IV, CPU times for one iteration are as shown in Table I.

VI. SUMMARY

In clinical applications of fluorescence tomography, appropriately regularized nonlinear least-squares inversion strategies may be required for accurate image reconstruction [5]. These methods require repeated and computationally expensive computation of the Jacobian sensitivities. For successful clinical translation of the method, it is important to determine a method

for sensitivity calculation that is both accurate and as computationally efficient as possible. Finite-difference approximations to the Jacobian can be accurate, but require careful determination of increment sizes and are computationally prohibitive on large problems [33]. Exact adjoint sensitivities [33] are accurate and computationally feasible, but are still the most computationally intensive aspect of the reconstruction algorithm. The introduction of additional assumptions can speed up computations of the adjoint sensitivities, but with the risk that the resulting approximations may have a negative impact on the quality of reconstructed images. Ideally, we would like to identify which assumptions, if any, can be made without significiant reduction in accuracy, in order to decrease computation times.

The exact adjoint sensitivity formulation of emission fluence with respect to fluorescence absorption is shown to comprise three terms. The first term reflects the sensitivities of diffusion and decay at the emission wavelength and is shown to make only a minor contribution to the overall sensitivity. We propose that omitting this term from the sensitivity calculations can save some computation time without introducing significant error into image reconstructions of fluorescence absorption. The second term reflects the sensitivities of diffusion and decay coefficients at the excitation wavelength; this term is shown to reduce the overall sensitivity, especially when large amounts of fluorophore are present in the target. Sensitivity approximations that omit this term overestimate the overall sensitivity, and this error has been shown to propagate into higher estimates of both volume and absorption value in fluorescence tomography for clinically relevant amounts of fluorophore, relative to estimates obtained when using the exact sensitivities. The third term reflects the sensitivity of the emission source term; although this term dominates the overall sensitivity, the relative value of Term 2 approaches that of Term 3 as target fluorophore increases in concentration or value. We conclude that using only the approximation of Term 3 [shown in term (12)], as proposed in [7]–[9], [12], and [25], may be too broad in its assumptions and may cause unacceptable errors in estimates of fluoresence absorption in some clinically relevant reconstructions, if quantitative estimates are sought. However, a more conservative adjoint approximation can be used without significant loss of accuracy. Specifically, we propose that an approximate formulation of sensitivities of emission fluence with respect to fluorescence absorption that includes terms reflecting the sensitivities of diffusion and decay coefficients at the excitation wavelength and of the emission source, as shown in (14), is sufficient for nonlinear least-squares approaches to fluorescence tomography

$$\delta\Phi_m \approx -\int_\Omega \left(\nabla\Psi_{xm}\frac{\partial D_x}{\partial \mu_{axf}}\delta\mu_{axf}\nabla\Phi_x - \Psi_{xm}\frac{\partial k_x}{\partial \mu_{axf}}\delta\mu_{axf}\Phi_x\right) + \int_\Omega \Psi_{mm}\frac{\partial \beta}{\partial \mu_{axf}}\delta\mu_{axf}\Phi_x. \quad (14)$$

Contributions from sensitivities of diffusion and decay coefficients at the emission wavelength can probably be safely ignored in clinical applications in order to speed up computation time. On the other hand, if the objective is simply to quickly identify the locations of targets, then using only Term 3 may be adequate. Even when seeking quantitatively accurate images, it may be reasonable to apply the more rapid approximation (9b) for the initial iterations and then switch to the more accurate approximation (approximate J) for fine tuning of the estimate.

This analysis only applies to sensitivities of emission fluence with respect to fluorescence absorption. When fluorescence tomography is employed to reconstruct other fluorescent properties, such as fluorescence lifetime, a similar analysis should be performed in order to determine which terms of (5) should be retained in the computation of the Jacobian sensitivities.

REFERENCES

[1] D. J. Hawrysz and E. M. Sevick-Muraca, "Developments toward diagnostic breast cancer imaging using near-infrared optical measurements and fluorescent contrast agents," *Neoplasia*, vol. 2, pp. 388–417, 2000.

[2] E. M. Sevick-Muraca, A. Godavarty, J. P. Houston, A. B. Thompson, and R. Roy, "Near-infrared imaging with fluorescent contrast agents," in *Handbook of Biomedical Fluorescence*, B. W.Brian W. Pogue and M.-A.Mary-Ann Mycek, Eds. New York: Marcel Dekker, 2003, pp. 445–527.

[3] M. J. Eppstein, D. E. Dougherty, T. L. Troy, and E. M. Sevick-Muraca, "Biomedical optical tomography using dynamic parameterization and Bayesian conditioning on photon migration measurements," *Appl. Opt.*, vol. 38, pp. 2138–2150, 1999.

[4] M. J. Eppstein, D. E. Dougherty, D. J. Hawrysz, and E. M. Sevick-Muraca, "Three-dimensional Bayesian optical image reconstruction with domain decomposition," *IEEE Trans. Med. Imag.*, vol. 20, pp. 147–163, Mar. 2001.

[5] M. J. Eppstein, D. J. Hawrysz, A. Godavarty, and E. M. Sevick-Muraca, "Three-dimensional, Bayesian image reconstruction from sparse and noisy data sets: near-infrared fluorescence tomography," in *Proc. Nat. Acad. Sci. USA*, vol. 99, 2002, pp. 9619–9624.

[6] A. Godavarty, M. J. Eppstein, C. Zhang, S. Theru, A. B. Thompson, M. Gurfinkel, and E. M. Sevick-Muraca, "Fluorescence-enhanced optical imaging in large tissue volumes using a gain modulated ICCD camera," *Phys. Med. Biol.*, vol. 48, pp. 1701–1720, 2003.

[7] J. Lee and E. M. Sevick-Muraca, "Fluorescence-enhanced absorption imaging using frequency-domain photon migration: tolerance to measurement error," *J. Biomed. Opt.*, vol. 6, pp. 58–67, 2001.

[8] ——, "Three-dimensional fluorescence enhanced optical tomography using referenced frequency-domain photon migration measurements at emission and excitation wavelengths," *J Opt. Soc. Amer. A*, vol. 19, pp. 759–771, 2002.

[9] M. A. O'Leary, D. A. Boas, B. Chance, and A. G. Yodh, "Reradiation and imaging of diffuse photon density waves using fluorescent inhomogeneities," *J. Luminescence*, vol. 60/61, pp. 281–286, 1994.

[10] J. Wu, Y. Wang, L. Perleman, I. Itzkan, R. R. Dasari, and M. S. Feld, "Time-resolved multichannel imaging of fluorescent objects embedded in turbid media," *Opt. Lett.*, vol. 20, pp. 489–491, 1995.

[11] J. Chang, R. L. Barbour, H. Graber, and R. Aronson, "Fluorescence optical tomography," *Proc. SPIE*, vol. 2570, pp. 59–72, 1995.

[12] M. A. O'Leary, D. A. Boas, X. D. Li, B. Chance, and A. G. Yodh, "Fluorescence lifetime imaging in turbid media," *Opt. Lett.*, vol. 21, pp. 158–160, 1996.

[13] D. Y. Paithankar, A. U. Chen, B. W. Pogue, M. S. Patterson, and E. M. Sevick-Muraca, "Imaging of fluorescent yield and lifetime from multiply scattered light reemitted from random media," *Appl. Opt.*, vol. 36, pp. 2260–2272, 1997.

[14] J. Wu, L. Perelman, R. R. Dasari, and M. S. Feld, "Fluorescence tomographic imaging in turbid media using early-arriving photons and Laplace transforms," in *Proc. Nat. Acad. Sci. USA*, vol. 94, 1997, pp. 8783–8788.

[15] J. Chang, H. L. Graber, and R. L. Barbour, "Improved reconstruction algorithm for luminescence when background luminophore is present," *Appl. Opt.*, vol. 37, pp. 3547–3552, 1998.

[16] H. Jiang, "Frequency-domain fluorescent diffusion tomography: a finite-element-based algorithm and simulations," *Appl. Opt.*, vol. 37, p. 5337, 1998.

[17] E. L. Hull, M. G. Nichols, and T. H. Foster, "Localization of luminescent inhomogeneities in turbid media with spatially resolved measurements of cw diffuse luminescence emittance," *Appl. Opt.*, vol. 37, pp. 2755–2765, 1998.

[18] V. Chenomordik, D. Hattery, I. Gannot, and A. H. Gandjbakhche, "Inverse method 3-D reconstruction of localized in vivo fluorescence—application to Sjogren syndrome," *IEEE J. Select. Topics Quantum Electron.*, vol. 54, pp. 930–935, 1999.

[19] R. Roy and E. M. Sevick-Muraca, "Truncated Newton's optimization scheme for absorption and fluorescence optical tomography: part II Reconstruction from synthetic measurements," *Opt. Exp.*, vol. 4, pp. 372–382, 1999.

[20] ——, "Active constrained truncated Newton method for simple-bound optical tomography," *J. Opt. Soc. Amer. A.*, vol. 17, pp. 1627–1641, 2000.

[21] Y. Yang, N. Iftimia, Y. Xu, and H. Jiang, "Frequency-domain fluorescent diffusion tomography of turbid media and in vivo tissues," *Proc SPIE*, vol. 4250, pp. 537–545, 2001.

[22] D. J. Hawrysz, M. J. Eppstein, J. Lee, and E. M. Sevick-Muraca, "Error consideration in contrast-enhanced three-dimensional optical tomography," *Opt. Lett.*, vol. 26, pp. 704–706, 2001.

[23] R. Roy and E. M. Sevick-Muraca, "Three-dimensional unconstrained and constrained image-reconstruction techniques applied to fluorescence, frequency-domain photon migration," *Appl. Opt.*, vol. 40, pp. 2206–2215, 2001.

[24] ——, "A numerical study of gradient-based nonlinear optimization methods for contrast-enhanced optical tomography," *Opt. Exp.*, vol. 9, pp. 49–65, 2001.

[25] V. Ntziachristos and R. Weissleder, "Experimental three-dimensional fluorescence reconstruction of diffuse media by use of a normalized Born approximation," *Opt. Lett.*, vol. 26, pp. 893–895, 2001.

[26] A. Thompson and E. M. Sevick-Muraca, "Near-infrared fluorescence contrast-enhanced imaging with intensified charge-coupled device homodyne detection: measurement precision and accuracy," *J. Biomed. Opt.*, vol. 8, pp. 111–120, 2003.

[27] S. Achilefu, H. N. Jimenez, R. B. Dorshow, J. E. Bugaj, E. G. Webb, R. R. Wilhelm, R. Rajagopalan, J. Johler, and J. L. Erion, "Synthesis, in vitro receptor binding, and in vivo evaluation of fluorescein and carbocyanin peptide-based optical contrast agents," *J. Med. Chem.*, vol. 45, pp. 2003–2015, 2002.

[28] A. Becker, C. Hessenius, K. Licha, B. Ebert, U. Sukowski, W. Semmler, B. Wiedenmann, and C. Grotzinger, "Receptor-targeted optical imaging of tumors with near-infrared fluorescent ligands," *Nat. Biotech.*, vol. 19, pp. 327–331, 2001.

[29] Y. Lin, R. Weissleder, and C.-H. Tung, "Novel near-infrared cyanine fluorochromes: synthesis, properties, and bioconjugation," *Bioconj. Chem.*, vol. 13, pp. 605–610, 2002.

[30] G. I. Marchuk, *Adjoint Equations and Analysis of Complex Systems*. Dordrecht, The Netherlands: Kluwer Academic, 1995.

[31] G. I. Marchuk, V. I. Agoshkov, and V. P. Shutyaev, *Adjoint Equations and Perturbation Algorithms in Nonlinear Problems*. Boca Raton, FL: CRC, 1996.

[32] S. R. Arridge, "Optical tomography in medical imaging," *Inv. Prob.*, vol. 15, pp. R41–R93, 1999.

[33] F. Fedele, J. P. Laible, and M. J. Eppstein, "Coupled complex adjoint sensitivities for frequency-domain fluorescence tomography: theory and vectorized implementation," *J. Comput. Phys.*, vol. 187, pp. 597–619, 2003.

[34] M. S. Patterson and B. W. Pogue, "Mathematical model for time-resolved and frequency-domain fluorescence spectroscopy in biological tissues," *Appl. Opt.*, vol. 33, pp. 1963–1974, 1994.

[35] E. M. Sevick-Muraca and C. L. Burch, "Origin of phosphorescence signals re-emitted from tissues," *Opt. Lett.*, vol. 19, pp. 1928–1930, 1994.

[36] C. L. Hutchinson, T. L. Troy, and E. M. Sevick-Muraca, "Fluorescence-lifetime determination in tissues or other scattering media from measurement of excitation and emission kinetics," *Appl. Opt.*, vol. 35, pp. 2325–2332, 1996.

[37] J. C. Ye, R. P. Millane, K. J. Webb, and T. J. Downar, "Importance of the ∇D terms in frequency-resolved optical diffusion imaging," *Opt. Lett.*, vol. 23, pp. 1423–1425, 1998.

[38] A. Godavarty, D. J. Hawrysz, R. Roy, E. M. Sevick-Muraca, and M. J. Eppstein, "The influence of the refractive index mismatch at the boundaries measured in fluorescence-enhanced frequency-domain photon migration imaging," *Opt. Exp.*, vol. 10, pp. 653–662, 2002.

[39] B. J. Tromberg, O. Coquez, J. B. Fishkin, T. Pham, E. R. Anderson, J. Butler, M. Chan, J. D. Gross, V. Venugopalan, and D. Pham, "Non-invasive measurements of breast tissue optical properties using frequency-domain photon migration," *Phil. Trans. Roy. Soc. Lond.*, vol. 352, pp. 661–669, 1997.

[40] J. S. Reynolds, T. L. Troy, and E. M. Sevick-Muraca, "Multipixel techniques for frequency-domain photon migration imaging," *Biotech Progress*, vol. 13, pp. 669–680, 1997.